Mathematical Framework of Tetramorphic MWCNT Configuration for VLSI Interconnect

Abu Bony Amin, *Graduate Student Member, IEEE,* and Muhammad Sana Ullah, *Senior Member, IEEE*

***Abstract*—Having a 1D material like Multiwall Carbon Nanotube (MWCNT) as a potential candidate for high speed Very Large Scale Integration (VLSI) interconnect creates a good scope to reduce the delay by estimating the parasitic elements i.e. Resistance (R), Inductance (L) and Capacitance (C) properly. We have contrived an innovative configuration namely Tetramorphic (TM) for the bundle of MWCNTs with four different diameters. We have focused on 45 nm, 22 nm, 11 nm and 7 nm technology nodes to justify the novelty of our proposed configuration over the existing MWCNT bundle configurations. Having the parasitic RLC elements for a specific technology node, the diameter optimization took place in this work. Subsequently, we obtain the propagation delay results for local, semi-global and global level interconnect. Finally, we compare the results with the other existing configuration to show the supremacy of our introduced configuration for MWCNT bundle to explore high speed VLSI interconnect and represent crosstalk delay and power dissipation. Moreover, this configuration is highly dense which will offer the size shrinkage feature in a substantial manner.**

***Index Terms*—Interconnects, multiwall carbon nanotube, propagation delay, very large scale integration, tetramorphic configuration.**

I. Introduction

EVER thriving concern about speed and size shrinkage [1] makes the researcher to probe further about the suitability of different 1D materials for high speed VLSI interconnect [2]. Contemporary research reveals the fact that the devices are becoming faster than the interconnect [3]. Eventually, getting focused on interconnect to reduce the propagation delay and attaining the most competent replacement of *Cu* based interconnect is demand of this era due to the potential hindrances in *Cu* based interconnect regarding electromigration [4], [5], shorter mean free path [5]–[7], higher resistivity [5], [8], lower thermal and electrical conductivity [9] and larger crosstalk coupling noise [9].

MWCNTs composed of several concentric tubes rolled one over the other with diameters ranging from few nanometers to tens of nanometers [10]. MWCNTs are preponderantly metallic due the physical structure of the shells [11]–[13]. Metallic behavior of CNTs makes it a highly potential subject of VLSI interconnect as it yields high density of current ($> 1\times10^{10} A/cm^2$) without showing any electromigration [10], [11]. Besides this, it has been elucidated that variation in temperature bears upon the CNT and *Cu* based interconnects quite differently and a heterogeneous system of *Cu*/SWNT/MWNT yields the highest performance betterment for interconnects using the depicted model in [14]. The potentials of the mixed bundles are highlighted in [15] after developing the accurate conductance model for both MWCNTs and SWCNTs by pursuing a comparison study of the mixed CNT bundles and the standard copper interconnects. It is also shown in [16] that the temperature coefficient of resistance (TCR) is always positive and increases with length for SWCNT and MWCNT.

Though it has been claimed in [17] that MWCNT may have conductivity several times larger than that of copper or Single Wall Carbon Nanotube (SWCNT) bundles in case of longer length of a few hundreds of micrometers, densely packed SWCNT bundles shows more than two times higher conductivity compared to MWCNTs in case of shorter lengths of <10μm. Yet some perceptible works [1], [13], [18]–[20] on MWCNT bundle configuration has been conducted to enhance the reliability of interconnects in terms of propagation delay, crosstalk delay and power dissipation. Since it has already been shown in [21], [22] that Carbon Nanotube shows better performance than *Cu* based interconnects does in terms of propagation delay, we are going to focus on the configuration of CNT bundle to meet the densely packed arrangement and size shrinkage requirements along with better performance in terms of propagation delay. If we emphasize on the configuration of MWCNT or MWCNT composite bundle to enhance the performance, a noteworthy contribution has been made by [13], [18], [19], [23]–[26].

Most of the works [1], [10] on CNTs has considered the bundle with CNT of same size which is actually not feasible for CNT growth during fabrication [27]. Moreover, due to the use of CNTs of same size, a lot of space has been left unoccupied in these bundle configurations. In addition, the analysis of the equivalent RLC model [20], [28], [29] of MWCNT is compromised because of considering the mean free path as a constant value while it is a dependent variable and function of the diameter of the shells and temperature.

The aforementioned work on MWCNT illuminated our motivation to come up with a groundbreaking idea to enhance the performance of MWCNT further when we noticed that MWCNTs are convenient to fabricate without significant involvement of the chirality and density control [20]. It is important to notice that the resistance and the possibility of conduction of all the inner shells of the MWCNTs can be varied based on the differences in the fabrication [11]. As a requirement of our proposed approach, growing the CNTs at

Manuscript received April 20, 2020; revised August 03, 2020; accepted September 16, 2020. This research is the part of MS thesis work and partially supported by professional development fund from Florida Polytechnic University. The review of this paper was arranged by Associate Editor John T. W. Yeow.

A. B. Amin is with the Department of Electrical and Computer Engineering, Florida Polytechnic University, Lakeland, FL, 33805 USA (e-mail: abonyamin5908@floridapoly.edu).

M. S. Ullah is with the Department of Electrical and Computer Engineering, Florida Polytechnic University, Lakeland, FL, 33805 USA (e-mail: mullah@floridapoly.edu).

This article has been accepted for publication in a future issue of this journal, but has not been fully edited. Content may change prior to final publication. Citation information: DOI 10.1109/TNANO.2020.3026609, IEEE Transactions on Nanotechnology

TABLE I
INTERCONNECT PARAMETERS [13], [18].

Parameters(unit)	Technology node (nm)			
	45	22	11	7
Width (nm)	70	28	14	10.8
Thickness (nm)	140	56	28	21.6
V_{dd} (V)	1	0.8	0.7	0.6
No. of metal level	10	13	14	14
Aspect ratio (AR)	2	2	2	2
Average dielectric constant (ϵ_r)	2.2	2.3	2.59	2.7

predefined locations may be necessary which can be met by the alternative bottom-up process [10] where MWCNTs are first grown (using HF-CVD) at predefined locations, subsequently gap filled with oxide, and finally leveled. Moreover, it is recommended in [30] that a high quality fabrication process can make CNT suitable for interconnect by offering low-contact resistance, good direction and compatibility with CMOS technology. It is claimed in [27] that centrifugally classified nanoparticles as the most promising 'seeds' to adopt the diameter-selective growth of CNTs.

As an aftermath, the stupendous configuration for MWCNT bundle, the TM configuration, was brought forth to address the ever growing concern of size shrinkage and delay performance. Our main objective is to analyze the performance i.e. propagation delay of our proposed configuration for different interconnect length i.e. local (< 100μm), semi-global (> 100μm) and global (> 500μm) [31] with different technology nodes to concentrate on size scaling. To ensure the size shrinkage, we obtain optimized diameter of each isolated MWCNT and we compute the delay with this diameter subsequently. We claim the transcendence of TM configuration by showing the comparison of results with formerly developed configurations.

Gholipour et al. offered a semi-analytical model in [32], capable to estimate the propagation delay, based on the simulation results. Although this ***RC*** network based model is significantly faster compared to the simulation of the equivalent circuit model [32], analytical delay model for ***RLC*** interconnects, derived in [33], is capable to capture source-sink delays with higher accuracy compared to Elmore delay model and several times faster than simulation using SPICE.

The remnant of the write up has been organized in following manner. The theory and calculation to estimate the circuit elements i.e. Resistance, Inductance and Capacitance based on the proposed configuration, depicted in Fig. 1, of MWCNT bundle has taken place in Section II namely theory development. Subsequently, we have eked out the optimized diameter for specific technology node i.e. 45 nm, 22 nm, 11 nm and 7 nm in terms of delay efficiency in Section III. In Section III, we have also appended the delay estimation of local, semi-global and global interconnects for different technology nodes using this optimized diameter along with the crosstalk delay and power dissipation estimation. Having obtained the result, we brought in the comparison with the previously developed configuration. The conclusion by explaining the future work potentiality was ultimately drawn in Section IV.

TABLE II
DEFINITION OF PARAMETERS.

Parameters	Definitions
e	Charge of an electron
ϵ_0	Dielectric permittivity of free space
ϵ_{r}	Dielectric permittivity
$\hbar$	Planck's constant
μ	Magnetic permeability
δ	Van der Wall's gap- The distance maintained between adjacent MWCNTs and adjacent shells of MWCNTs.
τ	RLC delay
$N_{\frac{\text{channel}}{\text{shell}}}$	Number of channel per shell of MWCNT
$D_{\text{square}_{\text{max}}}$	Diameter of the outermost shell of the MWCNT inscribed in square in Fig. 2
$D_{\text{vertex}_{\text{max}}}$	Diameter of the outermost shell of the MWCNT mounted on vertex of square in Fig. 2
$D_{\text{triangle}_{\text{max}}}$	Diameter of the outermost shell of the MWCNT inscribed in triangle in Fig. 2
$D_{\text{right}_{\text{max}}}$	Diameter of the outermost shell of the MWCNT inscribed in right triangle in Fig. 2
D_{i}	Diameter of the i^{th} shell of any specific MWCNT
n_{square}	Number of shells in the square inscribed MWCNT
n_{vertex}	Number of shells in the vertex mounted MWCNT
n_{triangle}	Number of shells in the triangle inscribed MWCNT
n_{right}	Number of shells in the right triangle inscribed MWCNT
n_{c}	Number of squares in the horizontal direction
n_{r}	Number of squares in the vertical direction
N_{square}	Number of square inscribed MWCNTs in the bundle
N_{vertex}	Number of vertex mounted MWCNTs in the bundle
N_{triangle}	Number of triangle inscribed MWCNTs in the bundle
N_{right}	Number of right triangle inscribed MWCNTs in the bundle
$R_{\text{lump}_{\text{square}}}$	Lump resistance appeared in square inscribed MWCNTs
$R_{\text{lump}_{\text{vertex}}}$	Lump resistance appeared in vertex mounted MWCNTs
$R_{\text{lump}_{\text{triangle}}}$	Lump resistance in triangle inscribed MWCNTs
$R_{\text{lump}_{\text{right}}}$	Lump resistance in right triangle inscribed MWCNTs
$R_{\text{s}_{\text{square}}}$	Scattering resistance in the square inscribed MWCNTs
$R_{\text{s}_{\text{vertex}}}$	Scattering resistance in the vertex mounted MWCNTs
$R_{\text{s}_{\text{triangle}}}$	Scattering resistance in the triangle inscribed MWCNTs
$R_{\text{s}_{\text{right}}}$	Scattering resistance in right triangle inscribed MWCNTs
b_1, b_2	Coefficients of second-order transfer function
R_{bundle}	Overall resistance in the bundle of TM configuration
T_0	Realistic operating temperature
$T_{0.9}$	90% threshold delay
υ_{F}	Fermi velocity
C_{q}	Quantum capacitance
$C_{\mathrm{s}}(i+1,i)$	Shell-to-shell coupling capacitance between i^{th} and $(i+1)^{th}$ shells
$C_{\text{ESC}_{\text{square}}}$	Equivalent quantum capacitance including the inter-shell coupling capacitance of square inscribed MWCNT
$C_{\text{ESC}_{\text{vertex}}}$	Equivalent quantum capacitance including the inter-shell coupling capacitance of vertex mounted MWCNT
$C_{\text{ESC}_{\text{triangle}}}$	Equivalent quantum capacitance including the inter-shell coupling capacitance of triangle inscribed MWCNT
$C_{\text{ESC}_{\text{right}}}$	Equivalent quantum capacitance including the inter-shell coupling capacitance of right triangle inscribed MWCNT
$C_{\text{e}_{\text{vertex}}}$	Electrostatic capacitance of vertex mounted MWCNT
$C_{\text{e}_{\text{triangle}}}$	Electrostatic capacitance of triangle inscribed MWCNT
$C_{\text{e}_{\text{right}}}$	Electrostatic capacitance of right triangle inscribed MWCNT
$C_{\text{ESC}_{\text{bundle}}}$	Total capacitance of the bundle using TM configuration
C_{cm}	Inter-bundle coupling capacitance
$L_{\text{m}_{\text{square}}}$	Magnetic inductance of square inscribed MWCNT
$L_{\text{m}_{\text{vertex}}}$	Magnetic inductance of vertex mounted MWCNT
$L_{\text{m}_{\text{triangle}}}$	Magnetic inductance of triangle inscribed MWCNT
$L_{\text{m}_{\text{right}}}$	Magnetic inductance of right triangle inscribed MWCNT
$L_{\text{k}_{\text{square}}}$	Kinetic inductance of square inscribed MWCNT
$L_{\text{k}_{\text{vertex}}}$	Kinetic inductance of vertex mounted MWCNT
$L_{\text{k}_{\text{triangle}}}$	Kinetic inductance of triangle inscribed MWCNT
$L_{\text{k}_{\text{right}}}$	Kinetic inductance of right triangle inscribed MWCNT
L_{bundle}	Total inductance of the bundle using TM configuration
S_p	Inter-bundle distance

This article has been accepted for publication in a future issue of this journal, but has not been fully edited. Content may change prior to final publication. Citation information: DOI 10.1109/TNANO.2020.3026609, IEEE Transactions on Nanotechnology

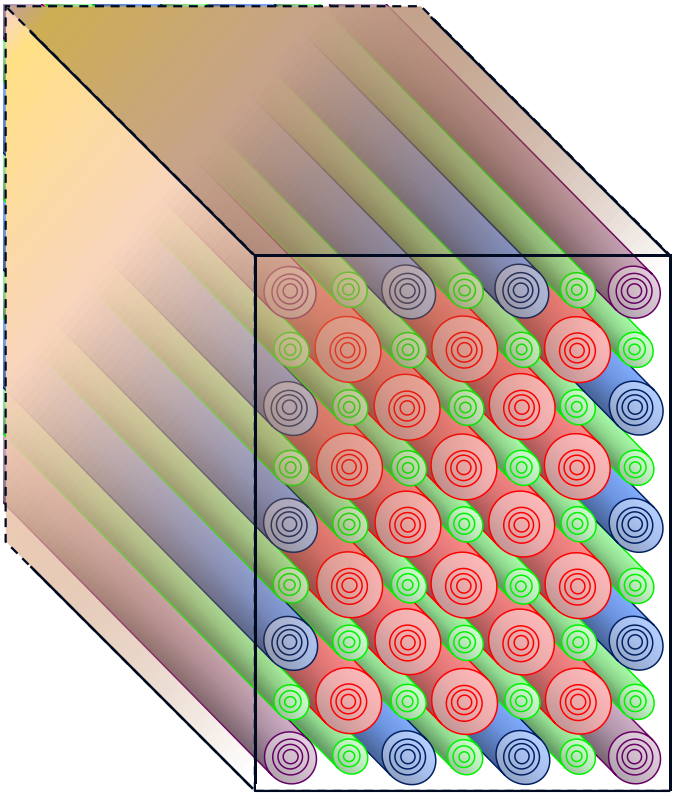

Fig. 1. Panoramic view of TM arrangement of bundle to show the original arrangement of MWCNTs horizontally by maintaining the size scalability and increasing the number of shells and MWCNTs in the bundle by maintaining proper distance δ.

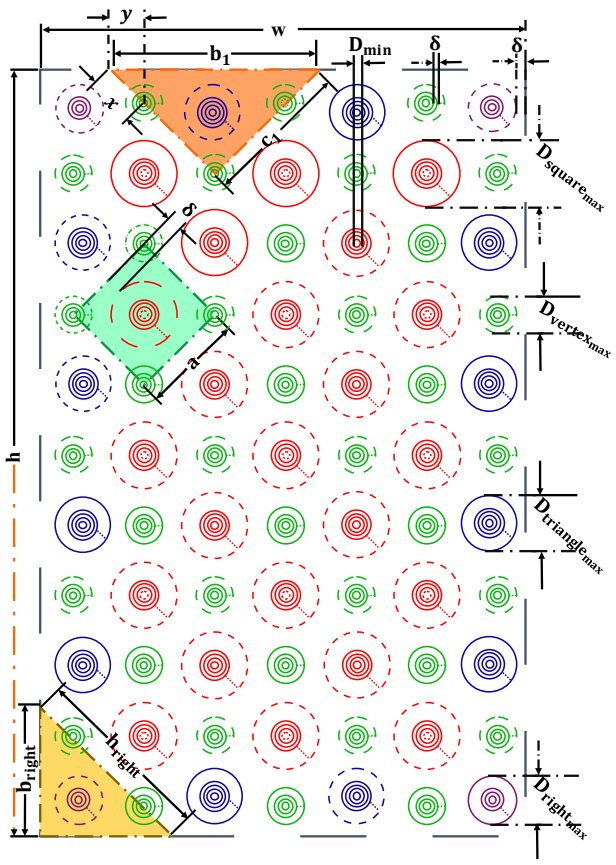

Fig. 2. Cross-sectional view of geometric representation of TM arrangement of MWCNT bundle having the MWCNT with four different diameters namely $D_{\text{square}_{\text{max}}}$, $D_{\text{vertex}_{\text{max}}}$, $D_{\text{triangle}_{\text{max}}}$ and $D_{\text{right}_{\text{max}}}$. MWCNTs with any size is intended to grow by keeping δ between adjacent MWCNTs and adjacent shells. Square, isosceles and right triangle is imagined to determine the the diameter of the inscribed MWCNTs conveniently.

II. Theory Development

Having got the bundle configurations, illustrated in [1], [34], evocative, we are going to expose the bundle configuration of MWCNT for emerging high speed interconnect. The main volition to design the configuration, depicted in Fig. 1, is to accommodate highest number of polymorphic MWCNT in given area for specific technology node. We will use Fig. 2 to determine the diameter of the MWCNTs of four different shapes. We address the red colored MWCNTs as square since those are inscribed in a transformed square, rotated by 45°, green colored MWCNT as vertex since those are mounted on the vertex of the square, blue colored MWCNTs as triangle as those are inscribed in isosceles triangle and violet colored MWCNTs as right since those are inscribed in right triangle. Before we introduce our mathematical framework that is developed for this TM configuration, we are representing the definition of used parameters in Table II.

Depending on the calculation, mentioned in [14], [17], [18], we can obtain the number of channel per shell of individual MWCNTs in following manner

$$N_{\frac{channel}{shell}} \approx \begin{cases} \alpha T D_i + \beta & \text{if } D_i > \frac{D_T}{T}; \\ \frac{2}{3} & \text{if } D_i \leq \frac{D_T}{T}; \end{cases} \tag{1}$$

where, $\alpha = 2.04\times10^{-4}\text{nm}^{-1}K^{-1}$, $\beta = 0.425$, $D_T = 1300\text{nm}\cdot K$.

At first, we will consider the side of the presumed transformed square, rotated by 45° and determine the outer-shell diameter of all MWCNTs in the bundle in terms of this side of the square as we can arbitrarily draw an square around the MWCNT with diameter $D_{\text{square}_{\text{max}}}$. We are going to consider the side of the square as parameter $'a'$ as shown in Fig. 2. So, the outermost shell diameter of the MWCNT, inscribed in square as follows.

$$D_{\text{square}_{\text{max}}} = a - 2\delta \tag{2}$$

According to [1], [13], [18], [35], δ should be maintained between two adjacent shells and adjacent MWCNTs.

$$D_{\text{vertex}_{\text{max}}} = a(\sqrt{2} - 1) \tag{3}$$

We can calculate x from Fig. 1 according to the following trigonometric formulae, $\sin 45° = \frac{1}{2x}\left(D_{\text{vertex}_{\text{max}}} + 2\delta\right)$. Hence,

$$x = a\left(1 - \frac{1}{\sqrt{2}}\right) \tag{4}$$

We can also calculate y from Fig. 1 according to the following trigonometric formulae, $\tan 45° = \frac{1}{2y}\left(D_{\text{vertex}_{\text{max}}} + 2\delta\right)$.

Hence,

$$y = \frac{a}{2}(\sqrt{2}-1) \tag{5}$$

Base of the isosceles triangle, illustrated in Fig. 1, can be reckoned using (6).

$$\begin{aligned} b_1 &= a\sqrt{2} + 2y \\ &= a(2\sqrt{2}-1) \end{aligned} \tag{6}$$

Other two legs with equal length can be determined using (7).

$$\begin{aligned} c_1 &= a + x \\ &= a\left(2 - \frac{1}{\sqrt{2}}\right) \end{aligned} \tag{7}$$

So, from (6) and (7), we can reckon the diameter of the inscribed MWCNT in the concerned isosceles triangle, depicted in Fig. 2.

$$\begin{aligned} D_{\text{triangle}_{\text{max}}} &= b_1\sqrt{\frac{2c_1 - b_1}{2c_1 + b_1}} \\ &= a(43 - 30\sqrt{2}) \end{aligned} \tag{8}$$

Hypotenuse of the right triangle can be obtained using (9).

$$\begin{aligned} h_{\text{right}} &= a + 2x \\ &= a(3 - \sqrt{2}) \end{aligned} \tag{9}$$

Since it is an isosceles right triangle, the base and height is of same length using (10).

$$\begin{aligned} b_{\text{right}} &= \frac{1}{\sqrt{2}}(a + 2x) \\ &= a\left(\frac{3}{\sqrt{2}} - 1\right) \end{aligned} \tag{10}$$

Finally, using (9) and (10), the outermost shell diameter of right triangle triangle inscribed can be calculated in (11).

$$\begin{aligned} D_{\text{right}_{\text{max}}} &= h_{\text{right}}\sqrt{\frac{2b_{\text{right}} - h_{\text{right}}}{2b_{\text{right}} + h_{\text{right}}}} \\ &= a(57 - 40\sqrt{2}) \end{aligned} \tag{11}$$

Number of shells in case of MWCNTs, inscribed in square (n_{square}), mounted on vertex(n_{vertex}), inscribed in triangle (n_{triangle}) and in right triangle (n_{right}), can be calculated using following formula (12) according to [13], [18], [35].

$$n = \left\lfloor \frac{D_{\text{max}} - D_{\text{min}}}{2\delta} \right\rfloor \tag{12}$$

To make our calculation regarding the number of MWCNT of different shapes easier, at first we are going to reckon the number of presumed transformed squares, rotated by 45°, in a bundle,

$$\text{Number of column, } n_{\text{c}} = \left\lfloor \frac{w - 2\delta - D_{\text{vertex}_{\text{max}}}}{\sqrt{2}a} \right\rfloor \tag{13}$$

$$\text{Number of row, } n_{\text{r}} = \left\lfloor \frac{h - 2\delta - D_{\text{vertex}_{\text{max}}}}{\sqrt{2}a} \right\rfloor \tag{14}$$

where, $\lfloor X \rfloor$ signifies that rounds each element of X to the nearest integer less than or equal to that element.

Now, we can determine the number of MWCNT, inscribed in the square, mounted on vertex, inscribed in the triangle and inscribed in right triangle using the expression (15), (16), (17) and (18) respectively.

$$\begin{aligned} N_{\text{square}} &= n_{\text{c}}n_{\text{r}} + (n_{\text{c}} - 1)(n_{\text{r}} - 1) \\ &= 2n_{\text{c}}n_{\text{r}} - n_{\text{c}} - n_{\text{r}} + 1 \end{aligned} \tag{15}$$

$$\begin{aligned} N_{\text{vertex}} &= n_{\text{c}}(n_{\text{r}} + 1) + (n_{\text{c}} + 1)n_{\text{r}} \\ &= 2n_{\text{c}}n_{\text{r}} + n_{\text{c}} + n_{\text{r}} \end{aligned} \tag{16}$$

$$\begin{aligned} N_{\text{triangle}} &= 2(n_{\text{c}} - 1) + 2(n_{\text{r}} - 1) \\ &= 2n_{\text{c}} + 2n_{\text{r}} - 4 \end{aligned} \tag{17}$$

$$N_{\text{right}} = 4 \tag{18}$$

Total number of polymorphic MWCNT in a bundle can be approximated by the sum of (15), (16), (17) and (18).

$$\begin{aligned} N_{\text{MWCNT}} &= N_{\text{square}} + N_{\text{vertex}} + N_{\text{triangle}} + N_{\text{right}} \\ &= 3n_{\text{c}}n_{\text{r}} + 2n_{\text{c}} + 2n_{\text{r}} + 1 \end{aligned} \tag{19}$$

A. Extraction of Parasitic Elements-Resistance

The lump resistance (R_{lump}), comprises the quantum or intrinsic resistance ($R_{\text{q}} = \frac{h}{2q^2} \approx 12.9\text{k}\Omega$), engendered by the quantum detainment of electrons in a nano-wire and imperfect metal-nanotube contact resistance (R_{mc}), may vary from few to several hundreds of kilo-ohms based on the fabrication process [1], [13], [18]. Now, we are going to reckon the lump resistance for different isolated MWCNTs of the proposed bundle configuration with polymorphic MWCNT using the following formulae, excerpted from [1], [3], [18], [19], [28], [35].

$$R_{\text{lump}} = \left[\sum_{i=1}^{n}\left(\frac{R_{\text{q}}}{2n_{\text{i}}} + R_{\text{mc}}\right)^{-1}\right]^{-1} \tag{20}$$

According to [18], the per unit length (p.u.l) scattering resistance (R_{s}) comes into consideration when length of the nano-wire surpasses the effective mean free path of the electron. Here, we are going to estimate the scattering resistance (R_{s}) for different isolated MWCNTs of the proposed bundle configuration with polymorphic MWCNT using the formulae, obtained from [1], [3], [18], [19], [28], [35].

$$R_{\text{s}} = \sum_{i=1}^{n}\frac{R_{\text{q}}}{n_{\text{i}}\lambda_{\text{i}}} \tag{21}$$

Since we are dealing with large mean free path (mfp) in the range of micrometers, to obtain the effective mfp (λ_{i}) for the i^{th} shell of any specific MWCNT by considering the conduction mechanism of MWCNTs as ballistic (lossless) [17], [18]. The overall mfp is represented in (22) as a function of temperature and diameter of any specific shell,

$$\lambda_{\text{i}} = \frac{10^3 D_{\text{i}}T_0}{T - 2T_0} \tag{22}$$

where, $T_0 = 100K$ and at room temperature, $T = 300K$.

B. Extraction of Parasitic Elements-Capacitance

In this section, p.u.l quantum capacitance (C_{q}), defined by the finite density of electronic states in a quantum wire [18] , is estimated by a recursive formulation because of the existence of coupling capacitance between two adjacent shells i.e. i^{th} and $(i+1)^{\mathrm{th}}$ shell i.e. $C_{\mathrm{s_{i+1,i}}}$ [1]. The calculation has been pursued for every isolated MWCNT and the final capacitance for TM bundle has been extracted.

$$C_{\mathrm{q}} = \frac{4e^2}{\hbar v_{\mathrm{F}}} \sum_{i=1}^{n} N_{\frac{\mathrm{channel}}{\mathrm{shell}}}(i) \tag{23}$$

where, $e = 1.6022\times10^{-19}C$, dielectric permittivity, $\epsilon_{\mathrm{r}} = 2.2$ and Fermi velocity, $v_{\mathrm{F}} = 8\times10^{5}\mathrm{ms}^{-1}$.

Here is the expression (24) for shell-to-shell coupling capacitance for isolated MWCNT in TM configuration [18], [20].

$$C_{\mathrm{s}}(i+1,i) = \frac{2\pi\epsilon_0\epsilon_{\mathrm{r}}}{\ln\left(\frac{D_{\mathrm{i}}+2\delta}{D_{\mathrm{i}}}\right)}, \{i \in \mathbb{N} : 1 \le i \le n\} \tag{24}$$

In the case of innermost shells, there is no shell-to-shell coupling capacitance. Hence, the equivalent capacitance expression should be as follows using (23) and (24) according to [1].

$$C_{\mathrm{ESC}}(1) = C_{\mathrm{q}}(1) \tag{25}$$

$$\begin{aligned} C_{\mathrm{ESC}}(i) =& C_{\mathrm{q}}(i) + C_{\mathrm{q-s}}(i-1) \\ & \text{where, } \{i \in \mathbb{N} : 2 \le i \le n\} \end{aligned} \tag{26}$$

$$\begin{aligned} C_{\mathrm{q-s}}(i-1) =& \left(\frac{1}{C_{\mathrm{ESC}}(i-1)} + \frac{1}{C_{\mathrm{s}}(i+1,i)}\right)^{-1} \\ & \text{where, } \{i \in \mathbb{N} : 2 \le i \le n\} \end{aligned} \tag{27}$$

Accordingly, we can obtain $C_{\mathrm{ESC_{vertex}}}(i)$, $C_{\mathrm{ESC_{triangle}}}(i)$ and $C_{\mathrm{ESC_{right}}}(i)$ for isolated vertex mounted, triangle inscribed and right triangle inscribed MWCNT. To obtain so, we will get required $C_{\mathrm{q_{vertex}}}(i)$, $C_{\mathrm{q_{triangle}}}(i)$, $C_{\mathrm{q_{right}}}(i)$, $C_{\mathrm{s_{vertex}}}(i+1,i)$, $C_{\mathrm{s_{triangle}}}(i+1,i)$ and $C_{\mathrm{s_{right}}}(i+1,i)$. Now, we can use (28) to obtain electrostatic capacitance (C_E).

$$C_{\mathrm{E}} = \frac{2\pi\epsilon_0\epsilon_{\mathrm{r}}}{\ln\left(\frac{D_{\mathrm{i}}+2\delta}{D_{\mathrm{i}}}\right)} \tag{28}$$

C. Extraction of Parasitic Elements-Inductance

Magnetic inductance engenders (L_m) by the magnetic field evoked from the current passing through a nanotube [18]. The following expression is for the isolated MWCNT in the TM configuration of the bundle.

$$L_{\mathrm{m}} = \frac{\mu}{2\pi}\cosh^{-1}\left(\frac{2h}{D_{\mathrm{i}}}\right) \tag{29}$$

The kinetic inductance (L_k) arises from the kinetic energy stored into the electrons [18]. In case of the TM model, the kinetic inductance for isolated MWCNT has been illustrated in following manner.

$$L_{\mathrm{k}} = \sum_{i=1}^{n} \frac{\hbar}{4e^2 v_{\mathrm{F}} N_{\frac{\mathrm{channel}}{\mathrm{shell}}}(i)} \tag{30}$$

Having the aforementioned mathematical models of Resistance, Inductance and Capacitance for isolated MWCNT, the ultimate bundle *RLC* are expressed in (31), (32) and (33) respectively.

$$\begin{aligned} R_{\mathrm{bundle}} =& \left(\frac{N_{\mathrm{square}}}{R_{\mathrm{lump_{square}}}} + \frac{N_{\mathrm{vertex}}}{R_{\mathrm{lump_{vertex}}}} + \frac{N_{\mathrm{triangle}}}{R_{\mathrm{lump_{triangle}}}} + \frac{N_{\mathrm{right}}}{R_{\mathrm{lump_{right}}}}\right)^{-1} \\ & + l\left(\frac{N_{\mathrm{square}}}{R_{\mathrm{s_{square}}}} + \frac{N_{\mathrm{vertex}}}{R_{\mathrm{s_{vertex}}}} + \frac{N_{\mathrm{triangle}}}{R_{\mathrm{s_{triangle}}}} + \frac{N_{\mathrm{right}}}{R_{\mathrm{s_{right}}}}\right)^{-1} \end{aligned} \tag{31}$$

$$\begin{aligned} C_{\mathrm{ESC_{bundle}}} =& \left[\left(N_{\mathrm{square}}C_{\mathrm{ESC_{square}}} + N_{\mathrm{vertex}}C_{\mathrm{ESC_{vertex}}} + N_{\mathrm{triangle}}C_{\mathrm{ESC_{triangle}}} + N_{\mathrm{right}}C_{\mathrm{ESC_{right}}}\right)^{-1}\right. \\ & \left. + \left(n_{\mathrm{c}}C_{\mathrm{e_{vertex}}} + (n_{\mathrm{c}}-1)C_{\mathrm{e_{triangle}}} + \frac{N_{\mathrm{right}}}{2}C_{\mathrm{e_{right}}}\right)^{-1}\right]^{-1} \end{aligned} \tag{32}$$

$$L_{\mathrm{bundle}} = \left(\frac{N_{\mathrm{MWCNT_{square}}}}{L_{\mathrm{m_{square}}} + L_{\mathrm{k_{square}}}} + \frac{N_{\mathrm{MWCNT_{vertex}}}}{L_{\mathrm{m_{vertex}}} + L_{\mathrm{k_{vertex}}}} + \frac{N_{\mathrm{MWCNT_{triangle}}}}{L_{\mathrm{m_{triangle}}} + L_{\mathrm{k_{triangle}}}} + \frac{N_{\mathrm{MWCNT_{right}}}}{L_{\mathrm{m_{right}}} + L_{\mathrm{k_{right}}}}\right)^{-1} \tag{33}$$

III. Analysis and Discussion of Simulation Result

In this section, we are going to conduct diameter optimization to attain the possible highest number of shells in MWCNTs with four different sizes in TM configuration. As we know that the delay performance gets better when the number of shells in MWCNT increases [31], we are going to vary the diameter for every isolated MWCNT by changing the side of the transformed square (a), shown in Fig. 2, solely. The attained result for different technology nodes are illustrated in Table III, Table IV, Table V and Table VI. To complete these tables, we obtain the parameters from [36]. Subsequently, we have represented the result graphically.

TABLE III
VARIATION OF NO. OF SHELLS BASED ON ISOLATED MWCNT DIAMETER.

Value of a (nm)	Position of MWCNT	Diameter (nm)	No. of Shells
7.68	Square	5.64	5
	Vertex	3.18	2
	Triangle	4.40	3
	Right	5.04	4
7.68	Square	7.00	7
	Vertex	3.18	2
	Triangle	4.40	3
	Right	5.04	4
8.68	Square	8.00	9
	Vertex	3.59	2
	Triangle	6.57	6
	Right	5.70	5
9.68	Square	9.00	10
	Vertex	4.00	3
	Triangle	7.33	8
	Right	7.01	6
10.68	Square	10.00	12
	Vertex	4.42	3
	Triangle	8.08	9
	Right	7.01	7
11.68	Square	11.00	13
	Vertex	4.83	4
	Triangle	8.84	10
	Right	7.67	8

Having the optimized diameter, the RLC parasitic elements of the circuit of TM configuration using equivalent single conductor (ESC) model have been calculated. However, the derived mathematical model based on the physics of TM configuration has been used from the previous section to simulate and estimate the R, L and C.

Finally, we have compared the result of ours to the previously developed model and submitted the comparison in tabular format. Through this way, we attempted to solidify the ground of our work.

A. Selection of Optimized Number of Shells by Varying Diameters

To obtain a better performance with any specific node, having a very efficient configuration is very important. To fulfill this prerequisite, we set the parameter of the side of the transformed square (a) and varied the diameter of every isolated MWCNT using expression (2), (3), (8) and (11) accordingly. Consequently, the number of shells in every isolated MWCNT will be changed along with the diameter based on the derivation of (12).

The obtained results have been illustrated in Table IV, Table V, Table VI and Table VII for different technology nodes i.e. 7 nm, 11 nm, 22 nm and 45 nm respectively. It is apparent from Fig. 3 that the Resistance (R) keeps decreasing with the decrease of outer shell diameter regardless of technology node i.e 7nm, 11nm, 22nm and 45nm. Since, the number of shells increases due to the decrease of outer shell diameter, the resistance forms in parallel. Hence, the equivalent resistance becomes lower with the increase of number of shells in an isolated MWCNT and number of MWCNTs in a bundle.

In addition, it is noticeable from Fig. 5 that the inductance decreases with the number of MWCNTs in the bundle. We can

TABLE IV
NUMBER OF SHELL IN BUNDLE IN CASE OF 7 nm TECHNOLOGY NODE.

$D_{\text{square}_{\text{max}}}$ (nm)	Position	Local w=10.8 nm h=20.2 nm	Semiglobal w=21.8 nm h=43.6 nm	Global w=124.4 nm h=311.2 nm
		No. of MWCNTs	No. of MWCNTs	No. of MWCNTs
5.64	Square	1	-	-
	Vertex	6	-	-
	Triangle	1	-	-
	Right	1	-	-
7.00	Square	-	3	578
	Vertex	-	10	655
	Triangle	-	4	74
	Right	-	4	4
8.00	Square	-	3	417
	Vertex	-	10	484
	Triangle	-	4	64
	Right	-	4	4
9.00	Square	-	-	323
	Vertex	-	-	382
	Triangle	-	-	56
	Right	-	-	4
10.00	Square	-	-	254
	Vertex	-	-	307
	Triangle	-	-	50
	Right	-	-	4
11.00	Square	-	-	228
	Vertex	-	-	277
	Triangle	-	-	46
	Right	-	-	4

TABLE V
NUMBER OF SHELL IN BUNDLE IN CASE OF 11NM TECHNOLOGY NODE.

$D_{\text{square}_{\text{max}}}$ (nm)	Position	Local w=17.4 nm h=32.5 nm	Semiglobal w=35 nm h=70 nm	Global w=200 nm h=500 nm
		No. of MWCNTs	No. of MWCNTs	No. of MWCNTs
5.64	Square	2	-	-
	Vertex	7	-	-
	Triangle	2	-	-
	Right	4	-	-
7	Square	2	17	1558
	Vertex	7	32	1683
	Triangle	2	12	122
	Right	4	4	4
8	Square	-	14	1146
	Vertex	-	27	1255
	Triangle	-	10	106
	Right	-	4	4
9	Square	-	11	959
	Vertex	-	22	1058
	Triangle	-	8	96
	Right	-	4	4
10	Square	-	4	725
	Vertex	-	13	812
	Triangle	-	6	84
	Right	-	4	4
11	Square	-	3	599
	Vertex	-	10	678
	Triangle	-	4	76
	Right	-	4	4

This article has been accepted for publication in a future issue of this journal, but has not been fully edited. Content may change prior to final publication. Citation information: DOI 10.1109/TNANO.2020.3026609, IEEE Transactions on Nanotechnology

TABLE VI
NUMBER OF SHELL IN BUNDLE IN CASE OF 22NM TECHNOLOGY NODE.

$D_{square_{max}}$ (nm)	Position	Local w=35 nm h= 65nm	Semiglobal w=70 nm h=140 nm	Global w=400 nm h=1000 nm
		No. of MWCNTs	No. of MWCNTs	No. of MWCNTs
5.64	Square	14	-	-
	Vertex	27	-	-
	Triangle	10	-	-
	Right	4	-	-
7	Square	14	127	6426
	Vertex	27	162	6679
	Triangle	10	32	250
	Right	4	4	4
8	Square	11	95	5072
	Vertex	22	162	5297
	Triangle	8	28	222
	Right	4	4	4
9	Square	11	60	3933
	Vertex	22	85	4132
	Triangle	8	22	196
	Right	4	4	4
10	Square	3	53	3290
	Vertex	10	76	3471
	Triangle	4	20	178
	Right	4	4	4
11	Square	3	38	2678
	Vertex	10	59	2843
	Triangle	4	18	162
	Right	4	4	4

TABLE VII
NUMBER OF SHELL IN BUNDLE IN CASE OF 45NM TECHNOLOGY NODE.

$D_{square_{max}}$ (nm)	Position	Local w=70 nm h=130 nm	Semiglobal w=140 nm h=280 nm	Global w=800 nm h=2000 nm
		No. of MWCNTs	No. of MWCNTs	No. of MWCNTs
5.64	Square	5	-	-
	Vertex	2	-	-
	Triangle	3	-	-
	Right	4	-	-
7	Square	116	564	26463
	Vertex	149	637	26974
	Triangle	30	70	508
	Right	4	4	4
8	Square	86	452	20511
	Vertex	115	517	20962
	Triangle	26	62	448
	Right	4	4	4
9	Square	60	332	16618
	Vertex	85	389	17023
	Triangle	22	54	402
	Right	4	4	4
10	Square	53	263	13545
	Vertex	76	314	13912
	Triangle	20	48	364
	Right	4	4	4
11	Square	33	233	11353
	Vertex	52	280	11688
	Triangle	16	44	332
	Right	4	4	4

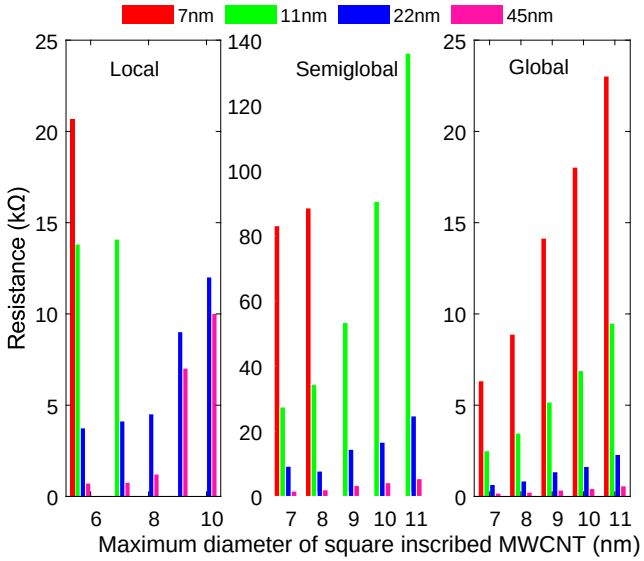

Fig. 3. Resistance of different technology nodes for local, semi-global and global interconnects for the TM configuration.

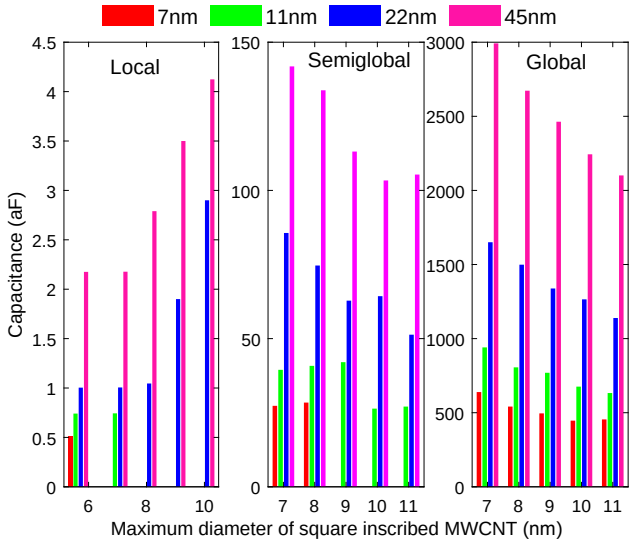

Fig. 4. Capacitance of different technology nodes for local, semi-global and global interconnects for the TM configuration.

estimate it from the expression (33) that the inductance forms the parallel combination among the MWCNTs. In contrast, it is lucid from Fig. 4 and (32) that the capacitance get increased while the number of MWCNTs is increasing in the bundle.

B. Delay Models for Optimized Situation with Different Technology Nodes

To come into a decision regarding the superiority of the proposed configuration of CNT bundle and materials in terms of delay, we have simulated the model using Kahng's delay model from [33]. A computationally easy, faster and more accurate analytical delay model, expressed in (34), is based on both first and second moments of the interconnect transfer function. The main reason behind to select the Kahng's model is to take the effect of inductance into account along with resistance and capacitance. Estimation of delay using Kahng's delay model is far accurate than that of using Elmore model and much faster than simulation using SPICE [33]. According to [33], the analytical RLC delay model for three different conditions i.e. real pole, complex pole and double pole as

This article has been accepted for publication in a future issue of this journal, but has not been fully edited. Content may change prior to final publication. Citation information: DOI 10.1109/TNANO.2020.3026609, IEEE Transactions on Nanotechnology

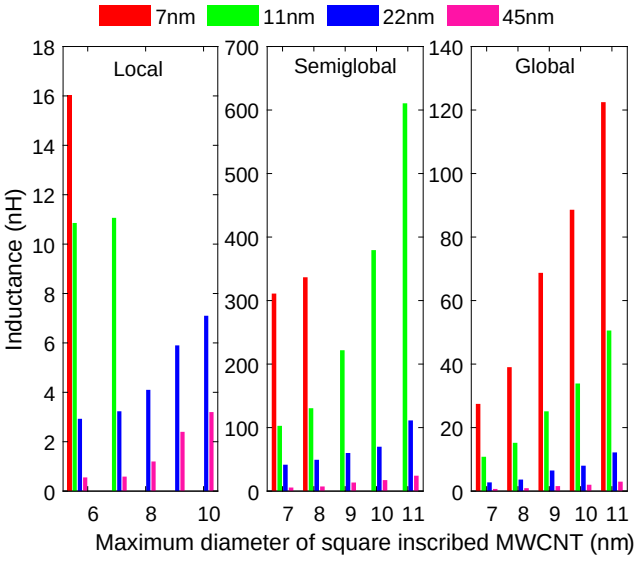

Fig. 5. Inductance of different technology nodes for local, semi-global and global interconnects for the TM configuration.

expressed in (34).

$$\tau = \begin{cases} 2.36\frac{2b_2}{b_1-\sqrt{4b_2-b_1^2}} & \text{if } (b_1^2-4b_2) \geq 0; \\ 1.66\frac{2b_2}{b_1-\sqrt{b_1^2-4b_2}} & \text{if } (b_1^2-4b_2) \leq 0; \\ \frac{2b_2}{b_1}\ln\left(10(1+\frac{2T_{0.9}}{b_1})\right) & \text{if } (b_1^2-4b_2) = 0. \end{cases} \quad (34)$$

where,

$$b_1 = R_d C_{ESC_{bundle}} + R_d C_T + \frac{R_{bundle} C_{ESC_{bundle}}}{2} + R_{bundle} C_T;$$

$$b_2 = \frac{R_d R_{bundle} C_{ESC_{bundle}}^2}{6} + \frac{R_d R_{bundle} C_{ESC_{bundle}} C_T}{6} + \frac{\left(R_{bundle} C_{ESC_{bundle}}\right)^2}{24} + \frac{R_{bundle}^2 C_{ESC_{bundle}} C_T}{6} + L_s C_{ESC_{bundle}} + L_s C_T + \frac{L_{bundle} C_{ESC_{bundle}}}{2} + L_{bundle} C_T;$$

and

$$T_{0.9} = 2.3\left[R_S(C_{ESC_{bundle}} + C_T) + R_{bundle} C_T\right] + 1.02 R_{bundle} C_{ESC_{bundle}}$$

It is observable from Fig. 6, Fig. 7 and Fig. 8 that with size shrinkage in terms of technology, the delay is increasing over time. The reason behind this characteristics is that the accommodated number of MWCNTs in a bundle is decreasing with technology scaling. It is also remarkable from Fig. 6 that in case of local interconnect, the propagation delay is the lowest for 45 nm technology node and keep increasing as technology is scaling down. Since width and height of the interconnect for higher technology nodes increase as illustrated in Table I, the area to accommodate more number of MWCNTs increases. We can observe from the expression (31), (32) and (33) that resistance and inductance keep increasing while capacitance goes down with increasing the number of

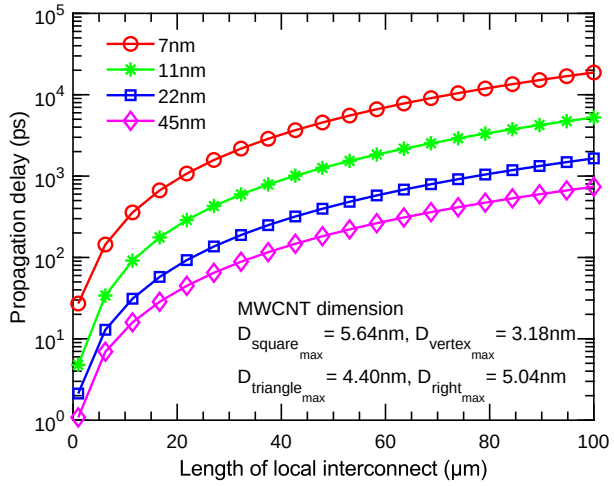

Fig. 6. Propagation delay of different technology nodes for local interconnect length.

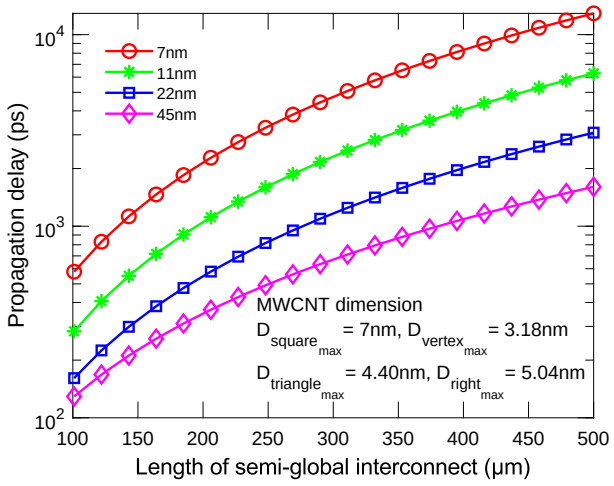

Fig. 7. Propagation delay of different technology nodes for semi-global interconnect length.

MWCNT in the bundle. Hence, this phenomena is obvious that the propagation delay, extracted using *RLC* from (34), will get decreased with increasing of number of MWCNTs in the bundle for all type of interconnect length (local, semi-global and global). The propagation delay for local, semi-global and global interconnect length has been depicted in Fig. 6, Fig. 7 and Fig. 8 respectively. It is apparent from all of these figures that delay is increasing with the length of the interconnect at any technology node.

C. Model Comparison

Here, we are going to show the comparison with the previously developed work [18] in tabular form. We prompted to reinforce that most of the individual component of *RLC* has been reduced in our case in a significant manner. The result has been shown in Table VIII. In the interest of obtaining *RLC* parameters, we approximated all components of resistance, inductance and capacitance. In this section, we are striving parasitic components for TM configuration with

This article has been accepted for publication in a future issue of this journal, but has not been fully edited. Content may change prior to final publication. Citation information: DOI 10.1109/TNANO.2020.3026609, IEEE Transactions on Nanotechnology

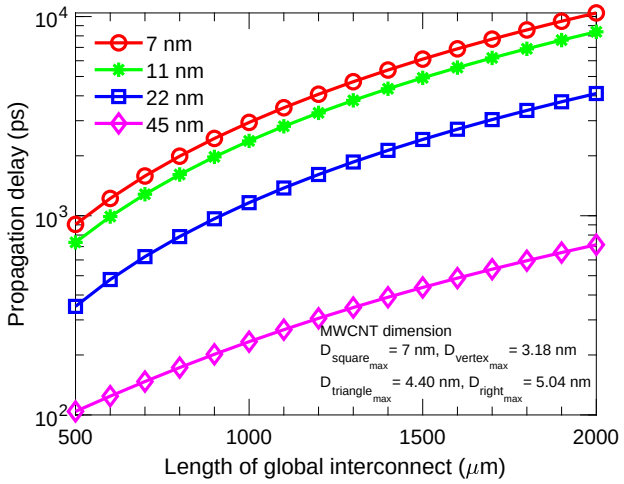

Fig. 8. Propagation delay of different technology nodes for global interconnect length.

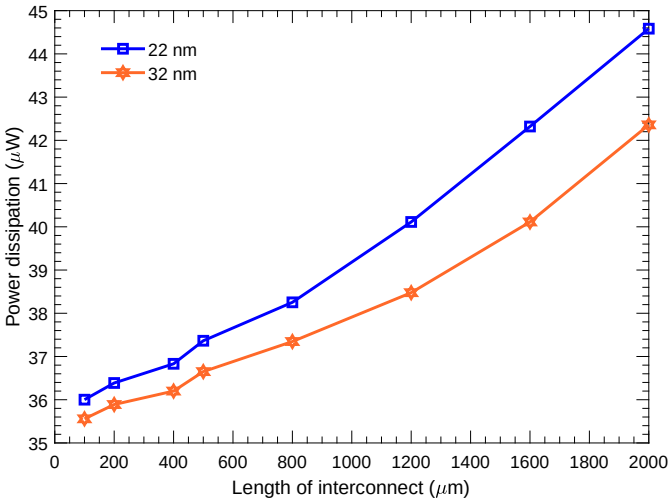

Fig. 10. Power dissipation of Tetramorphic configuration of MWCNT bundle for different technology nodes.

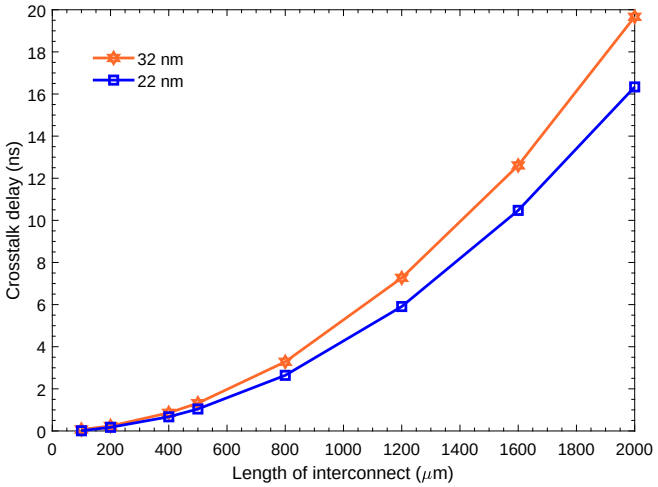

Fig. 9. Crosstalk delay of Tetramorphic configuration of MWCNT bundle for different technology nodes.

the previously developed configuration (MCB-VI), described as superior among six configurations in [18]. In case of resistance, we have calculated two components namely lump resistance (R_{lump}), shows 62.81% improvement, and scattering resistance (R_s), regresses by 5.06% which is insignificant, in TM configuration compare to MCB-VI. Between two components of inductance, kinetic inductance experiences 41.1% improvement along with magnetic inductance yields 14.05% betterment in TM configuration. In case of capacitance, the level of quantum capacitance is degraded by 31.33% while mutual capacitance is offering 7.18% improvement in TM configuration of the MWCNT bundle. Resistance and inductance is decreasing yet the capacitance is increasing because of increasing the number of MWCNTs in the bundle which can easily be evidenced from (31), (32) and (33). Hence, we can infer that the ultimate performance of TM configuration has been intensified in terms of delay as we have shown an overall significant improvement in RLC elements.

D. Crosstalk Delay and Power Dissipation

As it is remarked from [37], [38] that crosstalk is substantially affected by transition time of the signal, length of interconnect, spacing between interconnects, size of driver and receiver and line resistance, we are going to analyze the crosstalk delay with respect to length of the interconnect for 22 nm and 32 nm technology node using the driver resistance and inter-bundle capacitance as it is mentioned in [3] for comparison purpose.

The crosstalk delay has been engendered basically by the inter-bundle coupling capacitance (C_{cm}), primarily depends on the spacing (S_{p}) between aggressor and victim lines, which can be expressed using (35) obtained from [18].

$$C_{\mathrm{cm}} = \frac{\pi \epsilon_0 \epsilon_{\mathrm{r}}}{\cosh^{-1}\left(\frac{S_{\mathrm{p}}}{D_{\mathrm{n}}}\right)} n_{\mathrm{r}} \tag{35}$$

The performance of the proposed TM configuration is observed in Fig. 9 which indicates that the gap between 22nm and 32nm technology node is increasing while the interconnect length is going beyond the intermediate length. It is important to note that we accommodate approximately 3-5 times more MWCNTs in our TM configuration compare to [18] in the bundle. The comparison result is demonstrated in Table IX for consideration. It is also apparent from this table that TM configuration shows better performance in terms of crosstalk delay until global length interconnect.

The performance of the TM configuration is also limned in Fig. 10 to evaluate the power dissipation for 22nm and 32nm technology node which evidence that following technology node yields better performance. It is conspicuous from this figure that TM configuration dissipates almost same power as the configuration, illustrated in [18], does.

IV. Conclusion

The main intention of this work was to bring out a new architecture for the polymorphic MWCNTs in a bundle and

TABLE VIII
COMPARATIVE REPRESENTATION OF RLC ELEMENTS [19].

Interconnect Parasitics	MCB-I	MCB-II	MCB-III	MWB	MCB-IV	MCB-V	MCB-VI	Proposed	Improvement (%)
R_{lump} (kΩ)	3.22	3.20	3.20	3.20	3.21	3.21	3.20	1.19	62.81
R_s (Ω/μm)	1.28	1.13	1.04	0.85	1.02	1.02	0.79	0.83	-5.06
L_k (pH/μm)	2.84	2.12	2.6	1.99	2.54	2.72	1.21	1.04	14.05
L_M (pH/μm)	57.21	25.04	46.97	21.89	54.00	54.00	35.28	20.78	41.1
C_q (pF/μm)	1.09	1.46	1.19	1.55	1.21	1.21	0.83	1.09	-31.33
C_m (aF/μm)	342.34	584.84	584.84	62.83	325.93	325.93	62.83	58.32	7.18

TABLE IX
COMPARATIVE REPRESENTATION OF CROSSTALK DELAY.

Interconnect length (μm)	MMB-II (ns) [18]	MMB-III (ns) [18]	Tetramorphic (ns)	
			22 nm	32 nm
100	-	-	0.01	0.07
200	-	-	0.17	0.24
400	3.27	3.25	0.67	0.86
500	3.72	3.7	1.04	1.32
800	4.05	4	2.64	3.28
1200	4.65	4.6	5.91	7.27
1600	5.4	5.3	10.47	12.61
2000	6.25	6.1	16.34	19.67

establish this as a supreme one in terms of delay performance. We have established our proposed configuration namely TM configuration as the most sublime one by extracting the RLC parasitic elements in equivalent single line model and delay estimation accordingly. In this work, a comprehensive mathematical model to extract the R, L and C circuit elements for the TM configuration has been formulated. The diameter optimization is to come up with the optimized number of MWCNTs in our bundle configuration.

Finally, a comparison with previously reported result has been offered to reinforce our work. From the analysis, it can be inferred that our proposed model is highly suitable to resolve the growing concern of size shrinkage and speed in the field of high speed VLSI interconnect. It is believed that the resulting delay is a good estimation for an early stage analysis during the long iterative design and layout synthesis process of high-density ICs. The mathematical framework of this TM configuration can be embedded as a quick tool in the Computer Aided Design (CAD) flow of IC designs. Eventually, we would like to plumb the performance of this configuration for composite, mixture polymorphic carbon nanotube. Besides, this proposed configuration seems convincing to perform in highly scaled three-dimensional technology as Through Silicon Vias (TSV) [39]–[41].

REFERENCES

[1] M. Sahoo, P. Ghosal, and H. Rahaman, "Modeling and analysis of crosstalk induced effects in multiwalled carbon nanotube bundle interconnects: An abcd parameter-based approach," *IEEE Transactions on Nanotechnology*, vol. 14, no. 2, pp. 259–274, 2015.

[2] Y. Agrawal, M. G. Kumar, and R. Chandel, "A unified delay, power and crosstalk model for current mode signaling multiwall carbon nanotube interconnects," *Circuits, Systems, and Signal Processing*, vol. 37, no. 4, pp. 1359–1382, 2018.

[3] B. K. Kaushik and M. K. Majumder, *Carbon nanotube based VLSI interconnects: Analysis and design*. Springer, 2015.

[4] D. Rossi, J. M. Cazeaux, C. Metra, and F. Lombardi, "Modeling crosstalk effects in cnt bus architectures," *IEEE Transactions on Nanotechnology*, vol. 6, no. 2, pp. 133–145, 2007.

[5] A. Nieuwoudt and Y. Massoud, "Evaluating the impact of resistance in carbon nanotube bundles for vlsi interconnect using diameter-dependent modeling techniques," *IEEE Transactions on Electron Devices*, vol. 53, no. 10, pp. 2460–2466, 2006.

[6] D. Fathi and B. Forouzandeh, "A novel approach for stability analysis in carbon nanotube interconnects," *IEEE electron device letters*, vol. 30, no. 5, pp. 475–477, 2009.

[7] D. Das and H. Rahaman, "Modeling of single-wall carbon nanotube interconnects for different process, temperature, and voltage conditions and investigating timing delay," *Journal of Computational Electronics*, vol. 11, no. 4, pp. 349–363, 2012.

[8] K. Zhang, B. Tian, X. Zhu, F. Wang, and J. Wei, "Crosstalk analysis of carbon nanotube bundle interconnects," *Nanoscale research letters*, vol. 7, no. 1, p. 138, 2012.

[9] A. Bagheri, M. Ranjbar, S. Haji-Nasiri, and S. Mirzakuchaki, "Modelling and analysis of crosstalk induced noise effects in bundle swcnt interconnects and its impact on signal stability," *Journal of Computational Electronics*, vol. 16, no. 3, pp. 845–855, 2017.

[10] N. Srivastava and K. Banerjee, "Performance analysis of carbon nanotube interconnects for vlsi applications," in *ICCAD-2005. IEEE/ACM International Conference on Computer-Aided Design, 2005.* IEEE, 2005, pp. 383–390.

[11] Z. Kordrostami, M. H. Sheikhi, and R. Mohammadzadegan, "Modeling electronic properties of multiwall carbon nanotubes," *Fullerenes, Nanotubes, and Carbon Nonstructures*, vol. 16, no. 1, pp. 66–77, 2008.

[12] K. Singh and B. Raj, "Performance and analysis of temperature dependent multi-walled carbon nanotubes as global interconnects at different technology nodes," *Journal of Computational Electronics*, vol. 14, no. 2, pp. 469–476, 2015.

[13] K. S. Sandha and A. Thakur, "Comparative analysis of mixed cnts and mwcnts as vlsi interconnects for deep sub-micron technology nodes," *Journal of Electronic Materials*, vol. 48, no. 4, pp. 2543–2554, 2019.

[14] A. Naeemi and J. D. Meindl, "Performance modeling for single-and multiwall carbon nanotubes as signal and power interconnects in gigascale systems," *IEEE transactions on electron devices*, vol. 55, no. 10, pp. 2574–2582, 2008.

[15] S. Haruehanroengra and W. Wang, "Analyzing conductance of mixed carbon-nanotube bundles for interconnect applications," *IEEE Electron Device Letters*, vol. 28, no. 8, pp. 756–759, 2007.

[16] A. Naeemi and J. D. Meindl, "Physical modeling of temperature coefficient of resistance for single-and multi-wall carbon nanotube interconnects," *IEEE Electron Device Letters*, vol. 28, no. 2, pp. 135–138, 2007.

[17] A. Naeemi and J. D. Meindl, "Compact physical models for multiwall carbon-nanotube interconnects," *IEEE Electron Device Letters*, vol. 27, no. 5, pp. 338–340, 2006.

[18] M. K. Majumder, P. K. Das, and B. K. Kaushik, "Delay and crosstalk reliability issues in mixed mwcnt bundle interconnects," *Microelectronics Reliability*, vol. 54, no. 11, pp. 2570–2577, 2014.

[19] M. K. Majumder, B. K. Kaushik, and S. K. Manhas, "Analysis of delay and dynamic crosstalk in bundled carbon nanotube interconnects," *IEEE transactions on electromagnetic compatibility*, vol. 56, no. 6, pp. 1666–1673, 2014.

[20] H. Li, W.-Y. Yin, K. Banerjee, and J.-F. Mao, "Circuit modeling and performance analysis of multi-walled carbon nanotube interconnects," *IEEE Transactions on electron devices*, vol. 55, no. 6, pp. 1328–1337, 2008.

[21] A. B. Amin and M. S. Ullah, "Performance analysis of squarely packed polymorphic swcnt interconnect," in *2019 IEEE 10th Annual Ubiquitous Computing, Electronics & Mobile Communication Conference (UEMCON)*. IEEE, 2019, pp. 1199–1203.

[22] A. B. Amin and M. S. Ullah, "Performance analysis of squarely packed

dimorphic mwcnt bundle for high speed vlsi interconnect," 2020, to be published.

[23] S. Pasricha, F. Kurdahi, and N. Dutt, "System level performance analysis of carbon nanotube global interconnects for emerging chip multiprocessors," in *2008 IEEE International Symposium on Nanoscale Architectures*. IEEE, 2008, pp. 1–7.

[24] M. Sahoo and H. Rahaman, "Performance analysis of multiwalled carbon nanotube bundles," in *2013 IEEE XXXIII International Scientific Conference Electronics and Nanotechnology (ELNANO)*. IEEE, 2013, pp. 200–204.

[25] S. Subash, J. Kolar, and M. H. Chowdhury, "A new spatially rearranged bundle of mixed carbon nanotubes as vlsi interconnection," *IEEE Transactions on Nanotechnology*, vol. 12, no. 1, pp. 3–12, 2011.

[26] M. G. Kumar, Y. Agrawal, and R. Chandel, "Carbon nanotube interconnects- a promising solution for vlsi circuits," *IETE Journal of Education*, vol. 57, no. 2, pp. 46–64, 2016.

[27] T. Inoue, I. Gunjishima, and A. Okamoto, "Synthesis of diameter-controlled carbon nanotubes using centrifugally classified nanoparticle catalysts," *Carbon*, vol. 45, no. 11, pp. 2164–2170, 2007.

[28] M. S. Sarto and A. Tamburrano, "Single-conductor transmission-line model of multiwall carbon nanotubes," *IEEE Transactions on Nanotechnology*, vol. 9, no. 1, pp. 82–92, 2009.

[29] M. Majumder, N. Pandya, B. Kaushik, and S. Manhas, "Dynamic crosstalk effect in mixed cnt bundle interconnects," *Electronics letters*, vol. 48, no. 7, pp. 384–385, 2012.

[30] J. E. Morris and K. Iniewski, *Graphene, carbon nanotubes, and nanostructures: techniques and applications*. CRC Press, 2013.

[31] M. Kaur, N. Gupta, and A. Singh, "Impact of geometrical parameters on performance of mwcnt based chip interconnects," in *2017 Progress In Electromagnetics Research Symposium-Spring (PIERS)*. IEEE, 2017, pp. 988–993.

[32] M. Gholipour and N. Masoumi, "Efficient inclusive analytical model for delay estimation of multi-walled carbon nanotube interconnects," *IET circuits, devices & systems*, vol. 6, no. 4, pp. 252–259, 2012.

[33] A. B. Kahng and S. Muddu, "An analytical delay model for rlc interconnects," *IEEE Transactions on Computer-Aided Design of Integrated Circuits and Systems*, vol. 16, no. 12, pp. 1507–1514, 1997.

[34] K. S. Sandha and S. Sharma, "Performance analysis of different mixed-mwcnt structures as vlsi interconnects for nano-electronics ic design," *Journal of Nanoelectronics and Optoelectronics*, vol. 13, no. 3, pp. 357–367, 2018.

[35] D. Das and H. Rahaman, "Analysis of crosstalk in single-and multiwall carbon nanotube interconnects and its impact on gate oxide reliability," *IEEE Transactions on Nanotechnology*, vol. 10, no. 6, pp. 1362–1370, 2011.

[36] A. Ceyhan, "Interconnects for future technology generations-conventional cmos with copper/low-k and beyond," Ph.D. dissertation, Georgia Institute of Technology, 2014.

[37] B. K. Kaushik and S. Sarkar, "Crosstalk analysis for a cmos gate driven inductively and capacitively coupled interconnects," *Microelectronics Journal*, vol. 39, no. 12, pp. 1834–1842, 2008.

[38] B. K. Kaushik, S. Sarkar, R. Agarwal, and R. Joshi, "Crosstalk analysis and repeater insertion in crosstalk aware coupled vlsi interconnects," *Microelectronics International*, 2006.

[39] A. Kumari, M. Majumder, B. Kaushik, and S. Manhas, "Effect of polymer liners in cnt based through silicon vias," in *2014 IEEE 64th Electronic Components and Technology Conference (ECTC)*. IEEE, 2014, pp. 1921–1925.

[40] A. Alam, M. K. Majumder, A. Kumari, V. R. Kumar, and B. K. Kaushik, "Performance analysis of single-and multi-walled carbon nanotube based through silicon vias," in *2015 IEEE 65th Electronic Components and Technology Conference (ECTC)*. IEEE, 2015, pp. 1834–1839.

[41] B. K. Kaushik, V. R. Kumar, M. K. Majumder, and A. Alam, *Through Silicon Vias: Materials, Models, Design, and Performance*. Crc Press, 2016.

Abu Bony Amin received the B.S. degree in Electrical and Electronics Engineering from Chittagong University of Engineering and Technology, Chittagong, Bangladesh, in 2013.

He is currently working toward the M.S. degree in Electrical and Computer Engineering from Florida Polytechnic University, Lakeland, FL, USA, under supervision of Dr. Muhammad S. Ullah. His current research interest includes focusing on VLSI interconnect materials, mathematical model of different configuration of Carbon Nanotubes for high speed VLSI interconnect.

Amin was the recipient of the Best Paper Award at IEEE UEMCON 2019, Columbia University, NY, USA. He is also a graduate student member of the IEEE.

Muhammad Sana Ullah received the B.S. degree in electrical and electronic engineering from the Chittagong University of Engineering and Technology, Chittagong, Bangladesh, in 2008, the M.S. degree in electrical and computer engineering from Purdue University, Hammond, IN, USA, in 2013, and the Ph.D. degree in electrical and computer engineering from the University of Missouri–Kansas City, Kansas City, MO, USA, under the supervision of Dr. M. Chowdhury.

He joined the College of Engineering, Florida Polytechnic University, Lakeland, FL, USA, as an Assistant Professor of Computer Engineering. His current research interests include a relatively new methodology and nanotechnology for the next generation of computing and other micro- and nano-electronic applications, modeling of RLC interconnects and RF interconnect in high-density integrated circuits (ICs), investigation of a tunneling device based on transition metal dichalcogenide material, graphene, carbon nanotube, and other emerging 2-D nanomaterials, very large scale integration signal processing, and higher order statistics and spectra in signal processing.